Front. Earth Sci. 2020, 14(1): 25–36
https://doi.org/10.1007/s11707-019-0766-8

RESEARCH ARTICLE

Classification of mass-transport complexes and distribution of gashydrate-bearing sediments in the northeastern continental slope of the South China Sea

Chao FU (✉)[1], Xinghe YU (✉)[1], Xue FAN[2], Yulin HE[3], Jinqiang LIANG[3], Shunli LI[1]

1 School of Energy Resources, China University of Geosciences, Beijing 100083, China
2 Zhongyuan Gas Storage Company Limited, SINOPEC, Puyang 400083, China
3 Guangzhou Marine Geological Survey, Ministry of Land and Nature Resource, Guangzhou 510760, China

Abstract The drilling areas in Shenhu and Dongsha, South China Sea, studied from 2007 to 2015, reveal great heterogeneity in the spatial distribution of the gas hydrate reservoir. Various types of mass-transport complexes (MTCs) were developed in the study areas, which served as ideal reservoirs. To conduct exploration in these areas, it is necessary to study the different types of MTCs and the corresponding gashydrate accumulations. By integrating seismic reflection and log coring data, we classified three types of MTCs according to their stress distribution: the tension, extrusion, and shear types, and their corresponding gashydrate accumulation patterns. The results show that the accumulation of the gas-hydrate varies with the type of MTC and stress distribution depending on the MTC's position (e.g., in the headwall, translational, or toe areas). Owing to this variance of the MTC's position, the corresponding kinemics situation in the MTCs also varies. Accordingly, we determined the corresponding location in which the gashydrate develops for various types of MTCs. Based on the bottom simulating reflectors (BSRs) and the hydrate core and image logging data, the gashydrate reservoir shows an obvious heterogeneity in various types of MTCs. The gashydrate in the tension-type MTCs are mostly borne in the toe and the headwall parts. In extrusion-type MTCs, the translational and toe parts constitute an ideal hydrate reservoir. In shear-type MTCs, the headwall and toe parts' coarse-grained sediments show an obviously hydrate response. After comparing the gas-hydrate saturation and MTCs morphology statics data, we were able to quantitatively prove that the main factors determining gashydrate accumulation in the different types of MTCs are the fault displacement, sedimentary rate, and flow erosion rate.

Keywords gas hydrate, accumulation pattern, mass-transport complexes (MTCs), stress distribution, South China Sea

1 Introduction

Natural gas hydrates are quasi-ice crystalline compounds that are formed in a low-temperature and high-pressure environment and are comprised of water and natural gas (Guan et al., 2009; Matsumoto et al., 2011; Sha et al., 2015). The drilling results produced since 2015 in the northern slope of the South China Sea (SCS) have shown that mass-transport complexes (MTCs) are favorable reservoirs for gashydrate accumulation (Wang et al., 2014; Yu et al., 2014; Su et al.,2015; Zhong et al., 2017). Since the Miocene, the complex hydrodynamic settings in slope regions and canyon activity migration, introduced in Su et al. (2015 and 2017), have led to the development of many types of MTCs; this has made the investigation into the preservation of MTCs and their corresponding gashydrate-accumulation patterns challenging (Maslin et al., 1998; Rothwell et al., 1998; Mienert and Posewang, 1999; Milkov et al., 2000; Milkov et al., 2001 and 2012).

Previous studies have determined several parameters that affect the accumulation pattern of the different types of MTCs. In the study of Ulleung Basin in South Korea, the gas hydrate accumulation pattern in the reservoir was determined by grain-size, porosity, and lithological vertical sequence; thus, the reservoir heterogeneity played a significant role in the gas hydrate bearing (Horozal et al. 2009; Lee et al., 2012; Lee et al., 2013a). Mikov (2001) specified that the heat flow or geothermal fluctuation in the

Received November 15, 2018; accepted July 2, 2019

E-mails: chaofu@cugb.edu.cn (Chao Fu), billyu@cugb.edu.cn (Xinghe YU)

Gulf of Mexico can further lead to the release of gas hydrate in heterogeneous reservoirs. Additionally, studies on the gas hydrate content in MTCs have been conducted, particularly with respect to the free-gas release rate (Nguyen et al., 2016), the deposition rate (Riestenberg et al., 2003; Plaza-Faverola et al., 2012), and the effect of sea-level fluctuations (Maslin et al., 1998). Many published papers have noted that the complex sedimentary setting in the slope of the Pearl Mouth Basin in the SCS (Fig. 1) leads to multiple types of MTCs having developed in the study area (Zhu et al., 2010; Chen et al., 2014; Su et al., 2015; Zhou et al., 2015; Sun et al., 2018). Further, earlier studies classified the MTCs from a sedimentogenesis position (He et al., 2013; Sun et al., 2016), such as the fact that MTCs are rebuilt by contourites and triggered by gas hydrate releases. These studies focused on the microfaults and their impact on the heterogeneity of MTCs reservoirs. In this study, we select the Shenhu and Dongsha areas along the continental slope with various morphologies and different types of MTCs (Qikun et al., 2017).

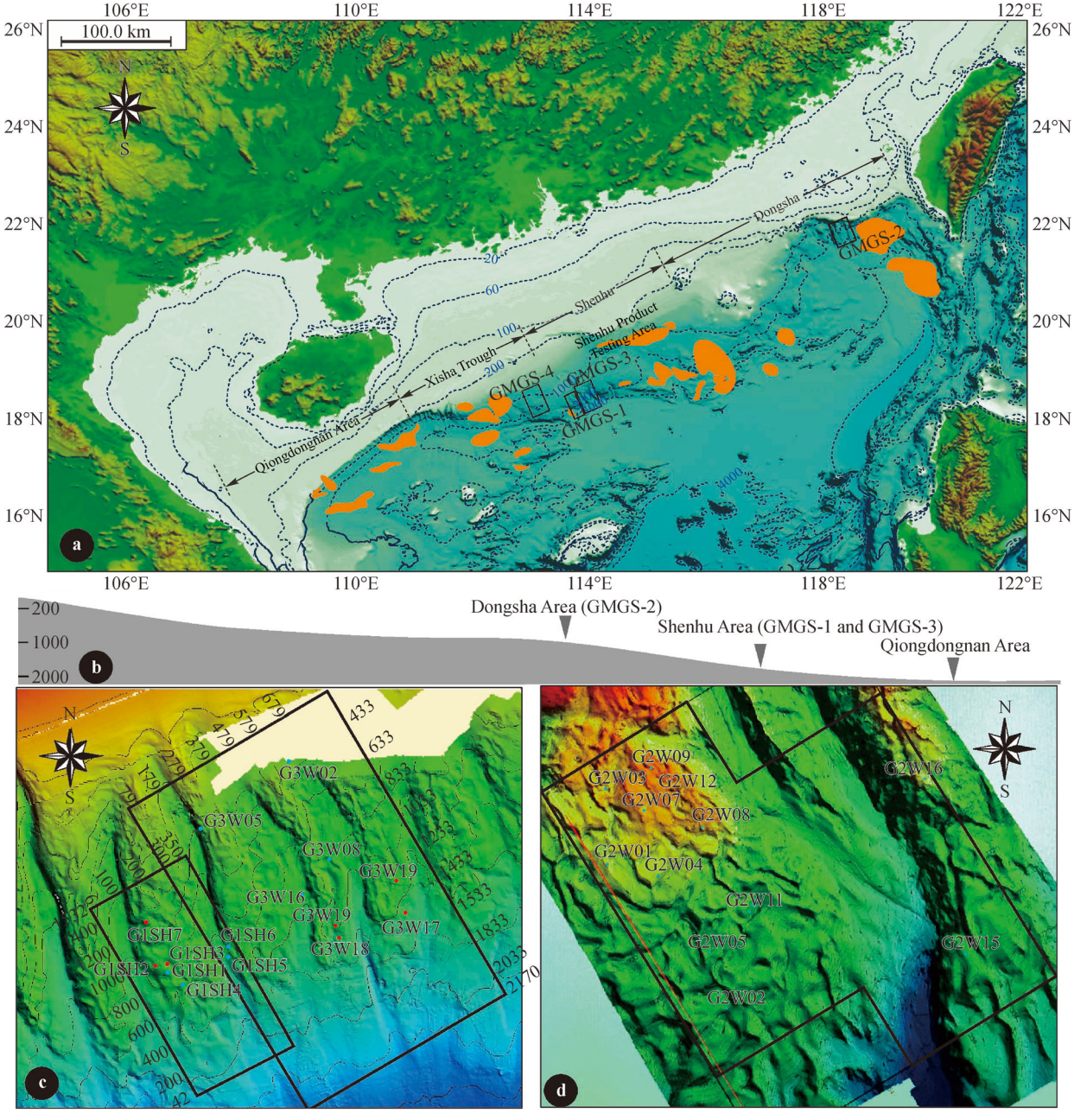

Fig. 1 Locations of the study areas. (a) The base map is the submarine geomorphologic map of the continental slope of the SCS. The two areas indicated in the map are the hydrate prospective areas: the Shenhu and Dongsha areas. The orange block in the map represents the hydrate-enriched area. The profile section (b) shows the relative locations of the Shenhu and Dongsha areas, and (c) and (d) are the multibeam geomorphology maps of Shenhu and Dongsha, respectively.

Referring to the retrogressive slide model employed by Kvalstad et al. (2005) and Alves et al. (2015), during the sediment unloading and shear band formation, we speculate on the gas hydrate accumulation pattern and its relationship with the MTCs distribution at various locations on the slope. In this study, we review previous literature and explain the differences in the gas hydrate distribution and content of various MTCs. By combining our results with those derived from the previous studies on MTCs stress distribution (Kvalstad et al., 2005; Bull et al., 2009; Alves, 2015), we divided the MTCs according to their kinematic setting. In the initial stage of the MTCs formation, they can be divided into three blocks: the over-steepened hand block, the translation block in the middle slope, and the folding and thrusting block in the lower slope (Bryn et al., 2005; Gee et al., 2005; Alves et al., 2010). Then, owing to the latter sedimentary process rebuilding, some blocks are eroded (Chen et al., 2014). We distinguish between the tension and extrusion-type MTCs according to the foliated strata or bookshelf sliding. Considering the influence of the bottom flow, the shear-type MTCs are identified by the obvious erosion boundary.

Previous studies mainly focused on the gas hydrate content of the MTCs, particularly the parameters affecting the accumulation system (Bünz et al., 2003; Shankar and Riedel, 2010; Sha et al., 2015): temperature, pressure, free gas, and targeted ideal reservoirs. However, studying the accumulation system and the hydrate-bearing pattern is difficult owing to the low seismic-data resolution and limited number of core samples with gas hydrate available in deep water (Lee and Collett, 2012; Lee et al., 2013a and 2013b). According to the hydrate-bearing pattern, the gas hydrates are categorized as fracture-filling and pore-filling (Cook et al., 2008; Riedelet al., 2008; Daigle and Dugan, 2010; Lee and Collett, 2012; Wang et al., 2013; Su, 2015; Su, 2017). However, the aforementioned patterns of hydrate accumulation developed areas remains confusing.

2 Geological setting and oceanographic frameworks

The Pacific, Eurasian, and Indo-Australian Plates directly control the formation and evolution of the SCS (Tang et al., 2017). The SCS was formed in the late Mesozoic, and it is based on the original SCS platform. The present tectonic framework of the northeastern continental slope is the result of unilateral extension, crustal fault depression, thinning, magmatic intrusion, and the formation of oceanic crust twice (Fig. 2).

The northern continental slope of the SCS has a geological environment and temperature and pressure conditions that are suitable for the development of hydrates; it is anticipated to have a good gas hydrate resource potential (Sha et al., 2015). Currently, many geological, geophysical, and geochemical abnormal characteristics related to gas hydrate have been described; four areas that are prospective sources of gas hydrates have been identified from the west to the east of the SCS (Fig. 1) as follows: two areas in Shenhu (GMGS-1 and GMGS-3),

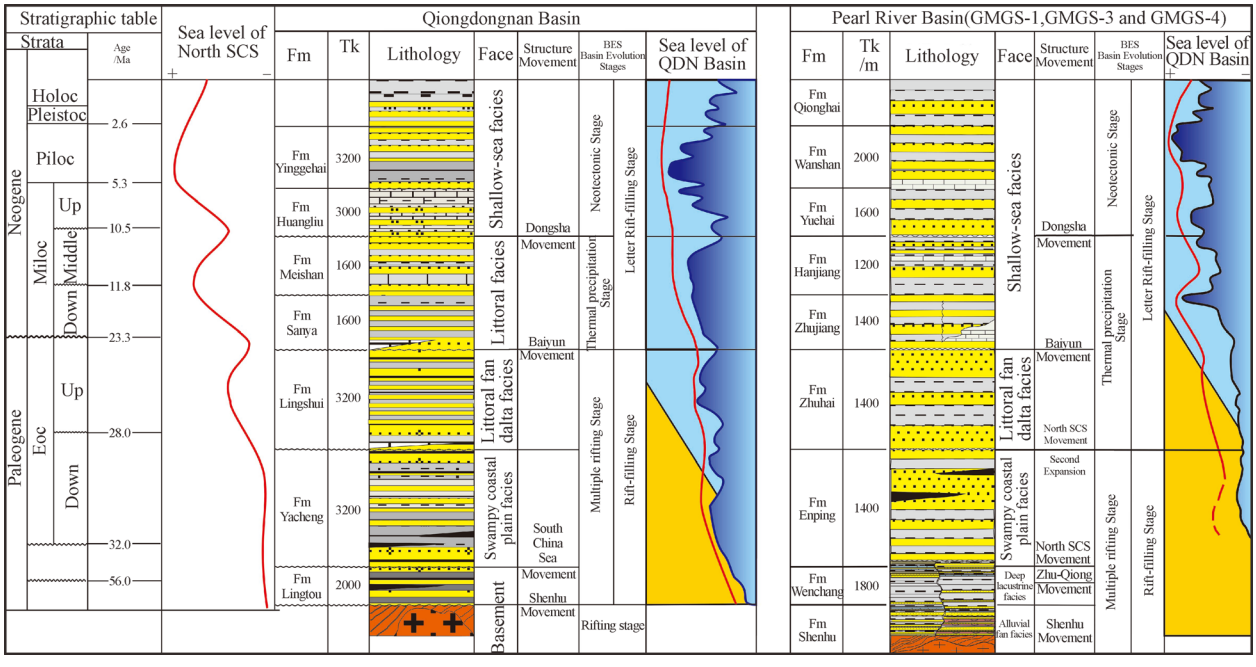

Fig. 2 Composite lithostratigraphic column of the Qiongdongnan, Shenhu, and Dongsha areas. The columns from right to left are as follows: formation, thickness, lithology, corresponding facies, and relative sea level. Fm = Formation, Tk = Thickness, Holoc = Holocene, Pleistoc = Pleistocene, Plioc = Pliocene, Mioc = Miocene, Oligoc = Oligocene, Eoc = Eocene.

one field in Dongsha (GMGS-2), and the Xisha Sea area (GMGS-4). This study mainly compares the development characteristics of the MTCs in the Shenhu and Dongsha areas.

The Shenhu Sea area, belonging to the Pearl River Mouth Basin, is located in the middle of the slope break belt and north of the SCS. It is the first area from which the gas hydrate samples were obtained. In this study area, the submarine topography fluctuates greatly and the continental slope topography is complex and changeable and declines in a ladder form on the whole. Sea troughs, valleys, hills, steep slopes, scarps, submarine plateaus, submarine slumps, and fans are all present in the study area; these favor the formation of hydrates. At water depths of 300–3400 m, hydrates occur at a small depth below the sea floor, and bottom simulating reflectors (BSRs) are found around the slumping blocks that develop widely and occur often in submarine MTCs.

The Dongsha area, belonging to the South-west Taiwan Basin, is located east of the slope break belt and in the northern part of the SCS. It covers an area of approximately 400 km^2. The drilling survey GMGS-2 revealed that the Dongsha drilling area has a great hydrate accumulation potential. The submarine topography is complex with large changes in the slopes, and the water depth is in the range of approximately 1,000–2,000 m. BSRs often occur around the MTC accumulation blocks.

3 Data and method

Cores, wire-line logs, and 3D seismic data were obtained in 2007 and 2015 from the Guangzhou Marine Geological Survey (GMGS). The core samples were collected along the slope, including GMGS-3-Well 11 (G3W11), GMGS-3-Well 17 (G3W17), GMGS-3-Well 18 (G3W18), and GMGS-3-Well 19 (G3W19). Image well-log data was collected in 27 wells (the well sites are shown in Fig. 1) as was their corresponding grain sizes. The size data were measured using the Mastersizer 2000, which is a laser particle-size analyzer (SYE209).

The pseudo three-dimensional (3D) survey data used in this study were taken from the GMGS from 2008 to 2009, with an average frequency of 65 Hz and 1-ms sampling interval for an approximately 15 $\times$ 25 km^2 area. The present study was principally based on the classical two-dimensional seismic facies analysis (section-view-based interpretation) and 3D seismic geomorphology approach (plan-view-based interpretation). The MTCs were recognized as lenticular-boundary shape seismic packages with a chaotic inner event by the corresponding seismic profile morphology (Fig. 3).

The log data used in this study were acquired by Fugro® and processed by Schlumberger® in 2015 and included the following parameters: natural gamma rays, gamma density, resistivity, and sonic velocity. The salt extraction effect of the gas hydrates, value of the resistivity log, and P-wave velocity were abnormally high in the shallow layers of the deep sea of the northeastern continental slope; thus, the GR curve was selected to represent the grain-size characteristics. The morphology of the GR curve was also selected as the reference of lithic-facies association.

To study the MTCs kinetics development, we reconstructed the paleo-morphology during the Wanshan Formation period (Fig. 2). We identified the fault (Figs. 4–6) and the geomorphology map (Figs. 7–9) using the Geoframe® software and released the erosion and compaction using the software Move®.

The original lithic-facies association may be altered or destroyed by later deposits; this should be taken into account in the lithic-facies association classification. We described the gas hydrate-bearing MTCs in the SCS following the classification criteria of Bouma et al. (1962) and Postma et al. (2015). Furthermore, we identified the relationship between the MTCs and seismic reflection data in reference to Bull (2009), and we integrated the core sample with the seismic data following the methodology of Zhong et al. (2017).

We distinguished the gas hydrate-bearing formation in the aforementioned nine wells; based on the pressure release in the core, we determined hydrate saturation in each well through in situ observation of the four core wells in Dongsha and Shenhu area. However, owing to the low number of wells in the GMGS-1, GMGS-2, and GMGS-3 areas (Fig. 1) and other restricting parameters, it was necessary to study and evaluate the seismic reflection characteristics of the gas hydrate-bearing layers to determine the hydrate distribution in the absence of data for the drilling area. By comparing the original sections with the synthetic seismograms of the high-resistivity regions, an amplitude anomaly was detected at the bottom of the gas hydrate-bearing layer (BGHSZ); this anomaly was attributed to free gas, which decreased the P-wave velocity. Nevertheless, BGHSZ appeared as a blank reflection band in the seismic profiles. The gas hydrate response in the BSR exhibited skewed reflection characteristics and an amplitude anomaly.

To study the stress distribution in various types of MTCs, we applied the geo-stress ellipsoid and ellipse method. According to the dip angle, grain size, and overlap compaction, we obtained broken angles. Furthermore, by incorporating the instantaneous frequency (IF) seismic attribute and its variance body attribute, the bearing pattern of the gas hydrate was revealed.

4 Mass-transport deposit classification and their sedimentary characteristics

We classified the MTCs based on Bull (2009) into tension, extrusion, and shear types (Fig. 3), which can be distinguished by the normal-fault development, location

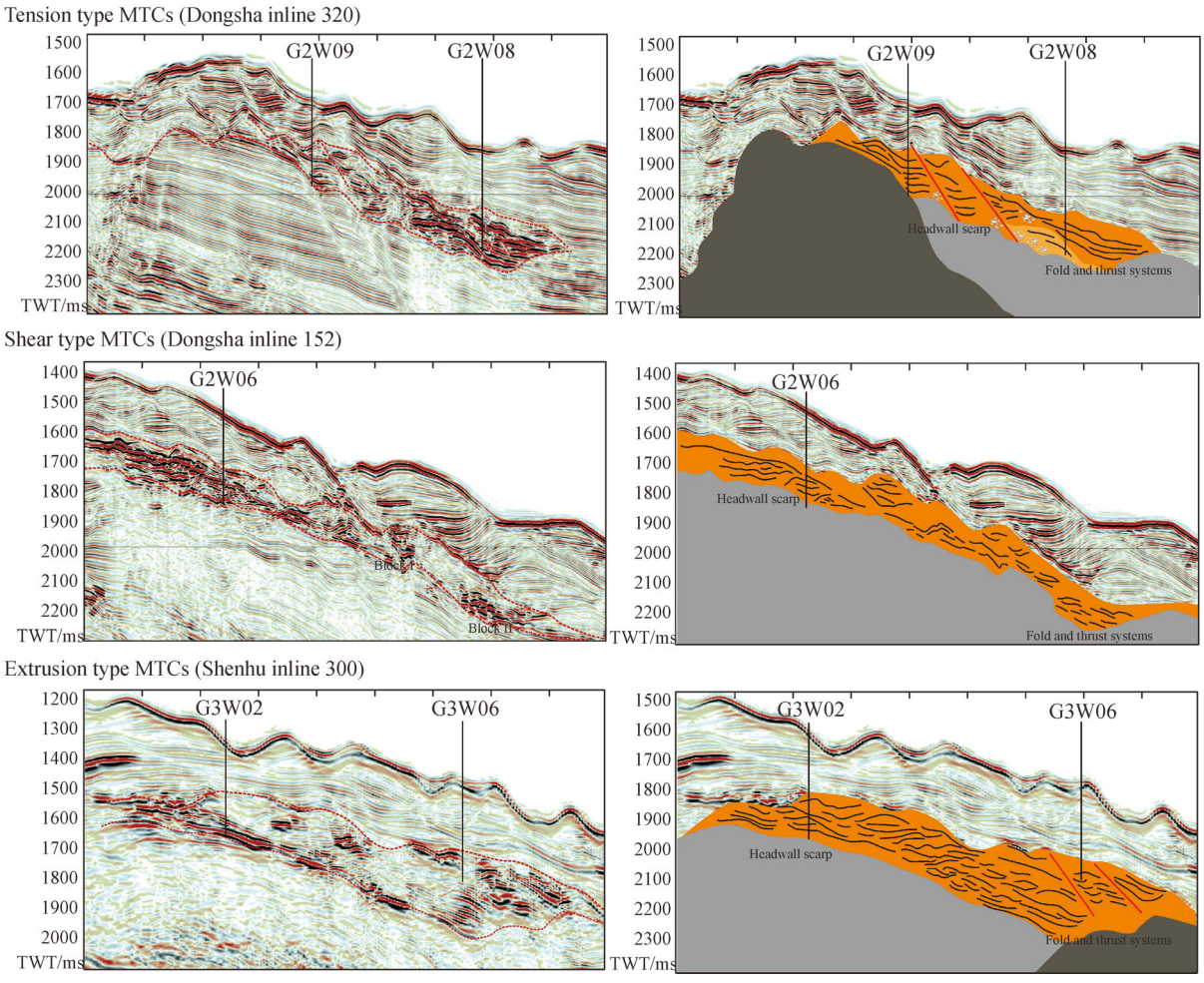

Fig. 3 The various types of MTCs are recognized from the seismic profile. In the tension-type MTCs, we can identify many normal faults in the headwall area. With the aid of the high seismic reflection, particularly for those parallel to the slope, we can recognize them as BSRs, which can reflect hydrate enrichment. Accordingly, we speculate that gas hydrate reservoirs in the tension-type MTCs, with low hydrate abundance, are mostly located at the toe and headwall parts. Regarding the extrusion-type MTCs, the translational and toe parts serve as desirable reservoirs for the gas hydrate accumulation. The shear-type MTCs' headwall and toe parts' coarse-grained sediment can contribute to the gas hydrate accumulation.

area, dip-angle difference, cover area, and other such characteristics. The criterion for the MTCs classification is as follows: tension type MTCs can be identified by some thrusting and internal folding (Dongsha in-line 320 in Fig. 3). The tension MTCs developed an obvious erosion boundary and the seismic event truncated in the middle translation parts (Shenhu in-line 152 in Fig. 3). The extrusion MTCs have characteristics such as the headwall scarp, extensional ridges, and developed blocks (Shenhu in-line 300 in Fig. 3).

4.1 Tension-type MTCs

As the profile and cross-section shown in Fig. 4(a), the headwall area in tension MTCs develops many normal faults owing to the high dip slope in the Dongsha area. This kind of MTC shows a clear-mound seismic package boundary (Figs. 4(b) and 4(c)). By combining this with the core sample observations, as in Zhong et al. (2017)'s study, the sediment can be divided into three layers (Fig. 4 (f)): the foraminifera-bearing hemipelagic deposits in the top layer, mass deposits with deformation structures in the middle layer, and fine-grain slump in the bottom layer. The fault in the middle area develops with a long break distance and it breaks the mound seismic package boundary (Fig. 4(d)). Impacted by the fault, the translational part of the MTC shows slumping and coarse-gained sediment developed. Based on the core observations, many fractures break the fine-grained slump owing to differing compaction in the toe.

4.2 Shear-type MTCs

As identified in the profile and cross-sections presented in Fig. 5(a), the thickness of the MTCs remains constant along the slope in the Dongsha area for shear type MTCs. It

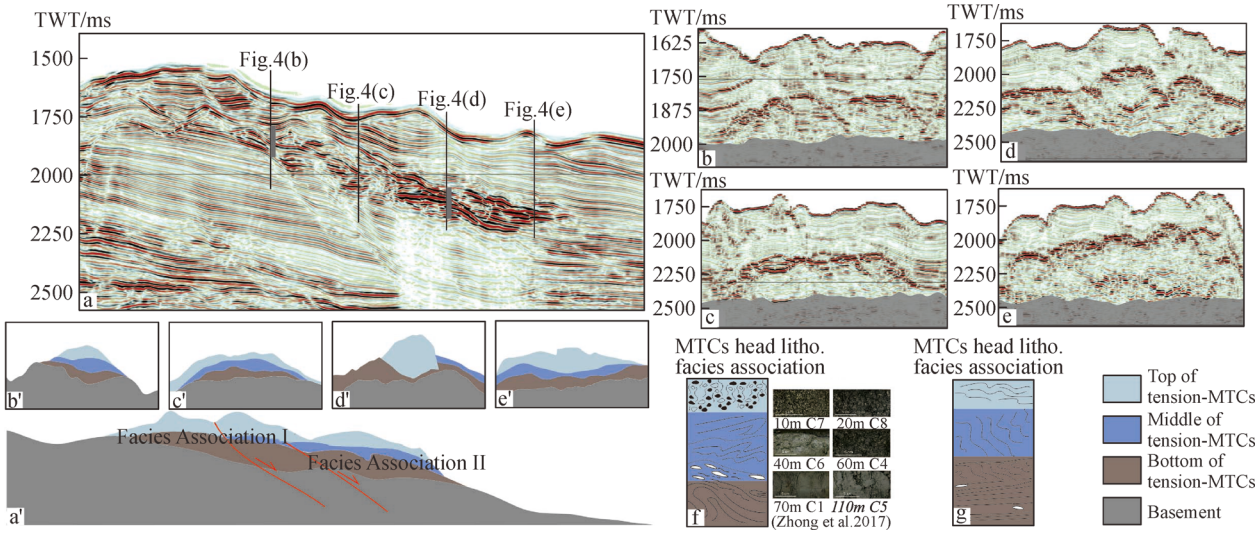

Fig. 4 The in-line seismic profile of the tension-type MTCs (a) and cross-line sections (b), (c), (d), and (e). (a') through(e') display the interpretation results, which reflect the different MTCs morphology along the slope. (f) and (g) show the identified lithofacies associations at different locations within the slope according to the studies of Bull (2009) and Zhong et al. (2017). According to the coring data of G2W09, the lithofacies in the toe area develop more fine-grained sump sediment than in the headwall area.

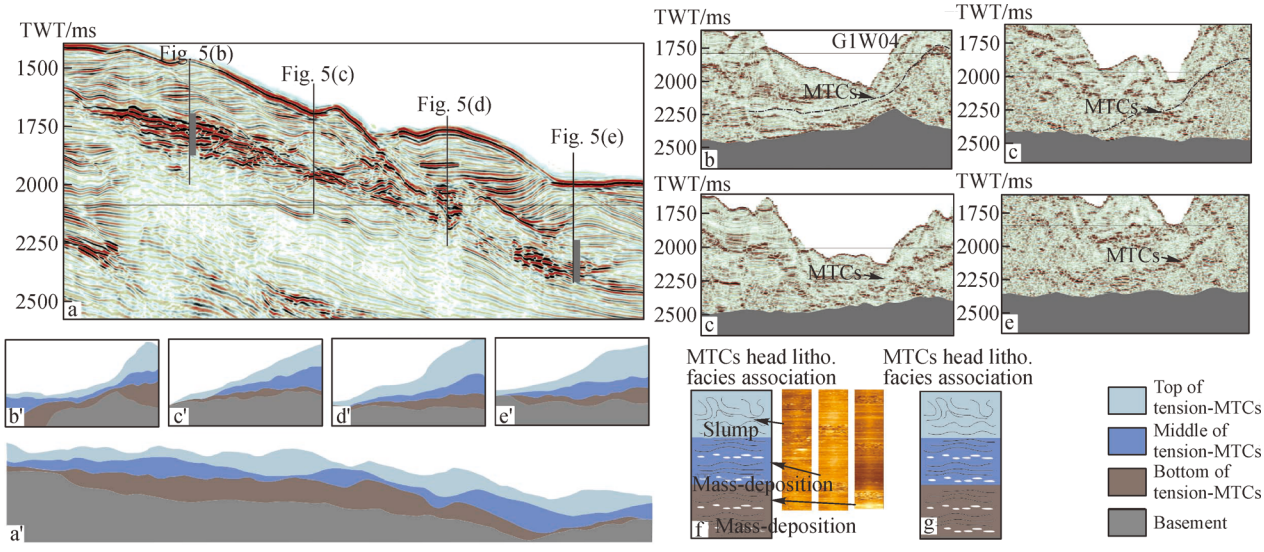

Fig. 5 The in-line seismic profile of tension MTCs (a) and cross sections (b), (c), (d), and (e). (a') through (e') display the interpretation results which reflect the different MTCs morphology along the slope. (f) and (g) show the identified lithofacies associations at different locations within the slope. Owing to the lack of core data, the lithofacies associations are shown using the resistivity image RAB.

displays an unclear wedge seismic package boundary (Figs. 5(b) and 5(c)). Combined with the image logging data, the sediment can further be divided into three layers (Figs. 5(f) and 5(g)): the foraminifera-bearing hemipelagic deposits in the top layer, mass deposits with deformation structures development in the middle layer, and the base layer. As identified from the low-continuity seismic reflection in the cross-sections (Figs. 5(b) and 5(c)), the reworked MTCs have low connectivity. Furthermore, we recognize several high-reflection blocks along the slope in the toe part. Thus, we presume this block has slid from the upper slope owing to bottom-flow reworking (similar to the sediment pattern observed by Sun et al. (2017)), and its lithofacies are the same as that of the upper-layer sediment.

4.3 Extrusion-type MTCs

As observed from the profile shown in Fig. 6, several thrust faults impact the morphology of the MTCs, particularly in the toe area. Without many normal faults in this area, the continual seismic package reflects the homogeneous reservoirs distribution in the headwall area. Moreover,

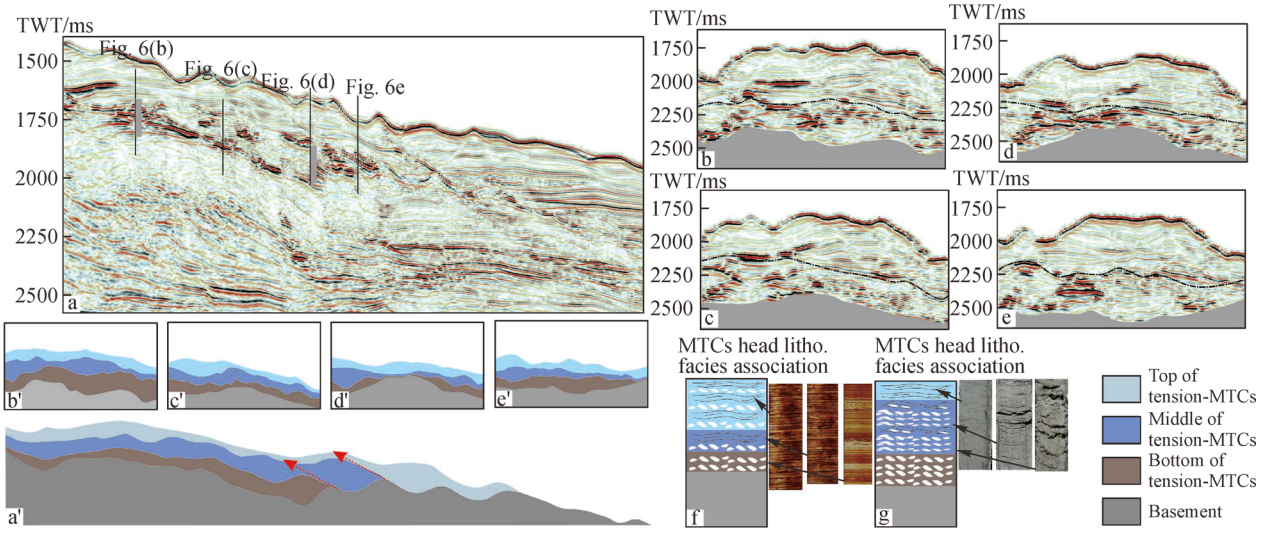

Fig. 6 The in-line seismic profile of the tension-type MTCs (a) and cross-line sections (b), (c), (d), and (e). (a') through (e') display the interpretation results which reflect the different MTCs morphology along the slope. (f) and (g) show the identified lithofacies associations at different locations within the slope.

the logging data display the mass sediment in this part. We identify many thrust faults that developed in the translational and toe areas, and the thickness of the MTCs increases sharply. In the core log, fractures are developed at the bottom and large pores are found in the top layer.

5 Mass-transport deposit kinematics and corresponding gas hydrate-bearing capacity

5.1 Mass-transport deposit Kinematics

Tension MTCs: The morphology (Fig. 7(a)) with a sharp dip angle suggests that several normal faults are developed in these MTCs along the slope (Figs. 7(b) and 7(c)). Accordingly, based on the aforementioned sediment characteristics and results of the failure envelope analyses, fractures are more conveniently developed in the coarse-grained upper slope deposits, whereas the fine-grained slumped toe part mainly develops intergranular pores.

Shear MTCs: The bottom flow (Fig. 8(a)) and tectonic setting in this area result in the formation of many faults with different directions that indica)te a shear setting (Figs. 8(b) and 8(c)). The failure envelope analyses indicate that fractures are more easily developed in the upper slope (Fig. 8(e)).

Extrusion MTCs: We identify a small uplift in the slope break area (Fig. 9(a)). Many thrust faults are developed in this block (Figs. 9(b) and 9(c)). The failure envelope analyses determine that fractures are developed in the headwall, transitional, and toe parts (Fig. 9(e)).

5.2 The relationship between MTCs and gas-hydrate distribution

Previous studies observed that hydrate melting leads to shear-strain generation and a decrease in the pore pressure, which make the former MTCs easier to rebuild (Maslin et al., 1998; Kvalstad et al., 2005). In the drilling area, the water depth ranges from 820 m to 1445 m and its values of heat flow range from 6 to 191 mW/m^2 with an average value of 76 mW/m^2. Thus, the development of the MTCs provided relatively appropriate temperature and pressure environment for the occurrence of the gas hydrate (Shi et al., 2003). A slip block might be an induction factor of the slump structure, or slumping might be the consequence of the resolution of gas hydrates (Brown et al., 2006). Submarine landslides are closely related to the development of gas hydrates. The factors that influence the formation of landslides mainly include the gradient ratio, provenance delivery volume, and sediment formation.

1) Tension MTCs. As stated above, we can classify the gas hydrates based on the patterns as fracture- and pore-filling gas hydrates. To the tension MTCs, in the headwall part, owing to the thickness of the mass deposits and high tensional stress, the coarse-grain sediment can form both pore- and fracture-filling reservoirs. In the translational and toe areas, normal faulting can provide a migration path for free gas. Covered by fine-grained sediment, these faults and their fractures can preserve gas hydrates when the temperature and pressure are suitable for gas hydrate bearing (Figs. 10(a) and 10(b)). In addition, if an amount of free gas is distributed through the fault or a gas chimney, this type of MTCs reservoir can bear both pore- and fracture-filling hydrates.

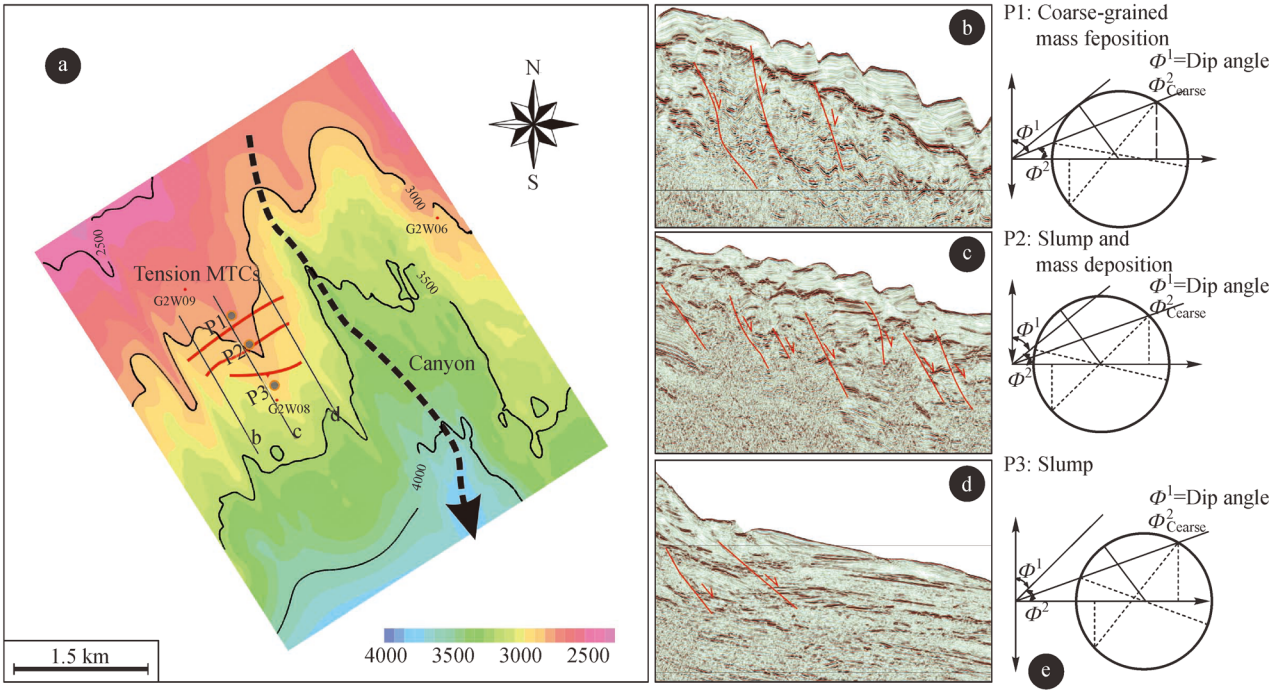

Fig. 7 Kinematics in the tension-type MTCs. The map shows the paleomorphology during the MTC's formation. (b)–(c) are the seismic profile cross-sections of the MTC, which show the fault structure and its dip angle, and (e) is the broken circle showing different points along the slope.

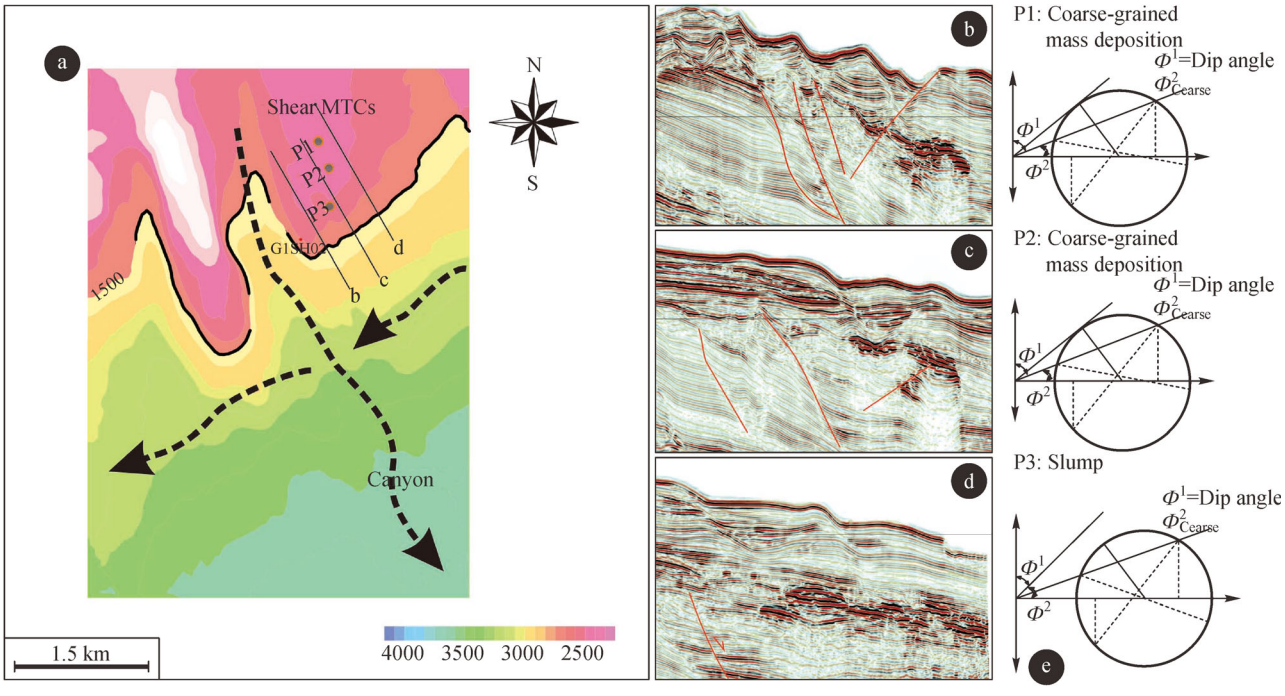

Fig. 8 Kinematics in the shear-type MTCs. The map displays the paleomorphology during the MTC's formation. (b)–(c) show the seismic profile cross-sections of the MTCs, which show the fault structure and its dip angle, and (e) is the broken circle showing different points along the slope.

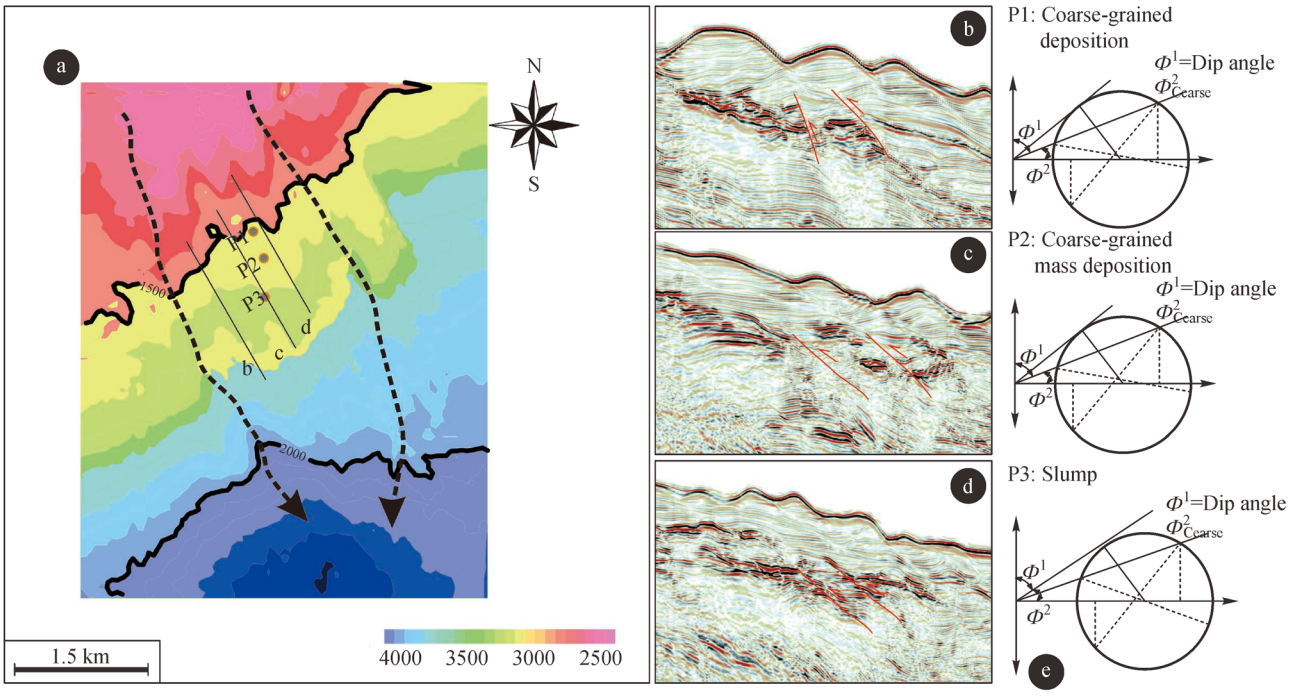

Fig. 9 Kinematics in extrusion-type MTCs. The map shows the paleomorphology during the MTC's formation. Owing to the small uplift at the MTCs' toe part, this type of MTCs develops thrust faults, as seen in (b)–(c), which show the fault structure and its dip angle. (e) is the broken circle showing different points along the slope.

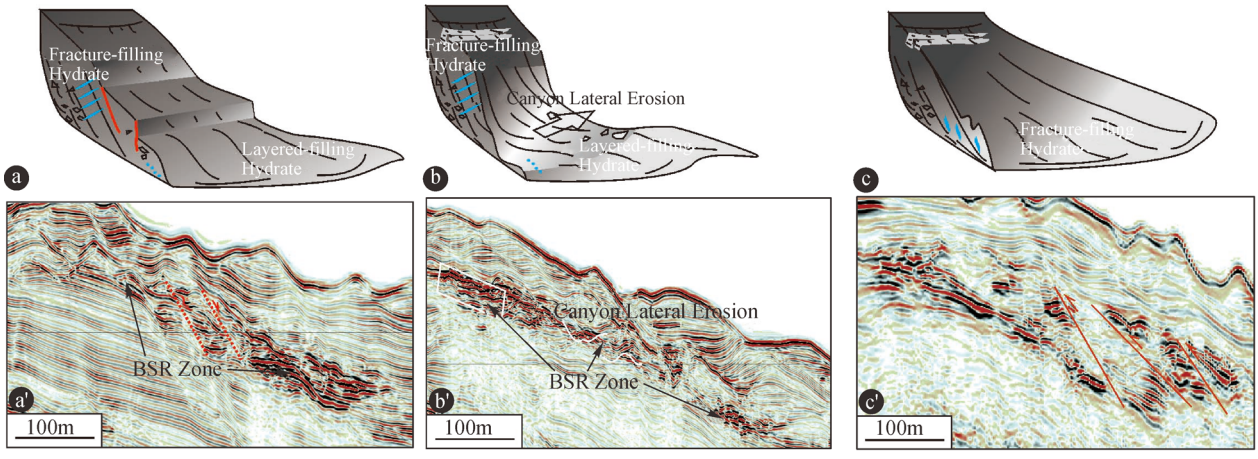

Fig. 10 The gas hydrate-bearing model of tension-type MTCs (a). The gas hydrate can be identified by the bottom simulation reflection (a'). The hydrate-bearing model of the shear-type MTCs (b). The gas hydrate can be identified by the bottom simulation reflection (b'). Gas hydrate-bearing model of the extrusion-type MTCs (c). The gas hydrate can be identified by the bottom simulation reflection (c').

2) Shear MTCs. There are several normal faults developed in this area despite the low stress experienced by it. With low external interference and ideal pressure-temperature conditions, the headwall in the shear-type MTCs can favor gas hydrate accumulation. In the translational and toe areas regarding the shear force stated above, the erosion caused by the bottom flow dissolves the free gas and leads to gas hydrate release. Therefore, several small coarse-grained blocks are expected along this type of MTCs; the translational and toe areas do not favor gas hydrate accumulation (Figs. 10(c) and 10(d)).

3) Extrusion MTCs. Similar to the aforementioned types of MTCs, small normal faults can be developed in the extrusion MTCs. Thus, the coarse-grain sediment can form both pore- and fracture-filling reservoirs. In the translational and toe areas, owing to the gravity along the slope and extrusion force caused by uplift, the thickness of the reservoir along the slope can favor thick pore-filling

reservoir formation (Figs. 10(e) and 10(f)). Meanwhile, the thrust faults and developed small fractures can provide free gas pathways. Accordingly, these parts of the MTCs can form thick gas hydrate reservoirs with both pore- and fracture-filling layers.

6 Impact factors of Gas Hydrate Accumulation and Corresponding Pattern

6.1 Temperature-Pressure fluctuations

The hydrate accumulation pressure is comprised of both hydrostatic and lithostatic pressure. The water depth ranges from 820 to 1445 m in the drilling area. In the northeastern continental slope of the SCS, the heat-flow value ranges from 6 to 191 mW/m^2, (average value = 76 mW/m^2). However, the difference in the MTCs preserved setting may lead to great head flow heterogeneity. As shown in Vadakkepuliyambatta et al. (2017)'s study in the Barents Sea, canyon migrations not only break the original MTC structure but also impact the local heat distribution, which may increase the heat-flow value on the sides of the canyon wall. Thus, owing to the lower impact of the later canyon activity, the pressure and temperature conditions of well-preserved MTCs are unaffected by the heat-flow fluctuation and its impact on the gas hydrate decomposition. However, owing to the later canyon activity leading to the MTC structure breakdown, which may change the original lithostatic pressure and its corresponding heat-flow distribution (He et al., 2013), the decomposition and release of the gas hydrate become easier.

6.2 MTCs Kinematic indicators and ideal reservoir distribution

Sedimentation rate: In previous studies, sedimentation rate is a key factor determining hydrate accumulation because of the reservoir space provided by mass deposition (Su et al., 2015 and 2017). The mass sediment provides the ideal pore and reservoir space for gas hydrate accumulation. Furthermore, the foraminifera in the reservoir can provide free gas, which accelerates the gas hydrate formation. Regarding the different types of MTCs, the coarse-grained mass sediment in the base layer of both the tension and shear MTCs can provide large porosity for gas hydrate bearing. With the fine-grained layer above the MTCs and ideal pressure-temperature conditions, these types of reservoirs favor the formation of the thickness pore-filling gas hydrates (Fig. 11).

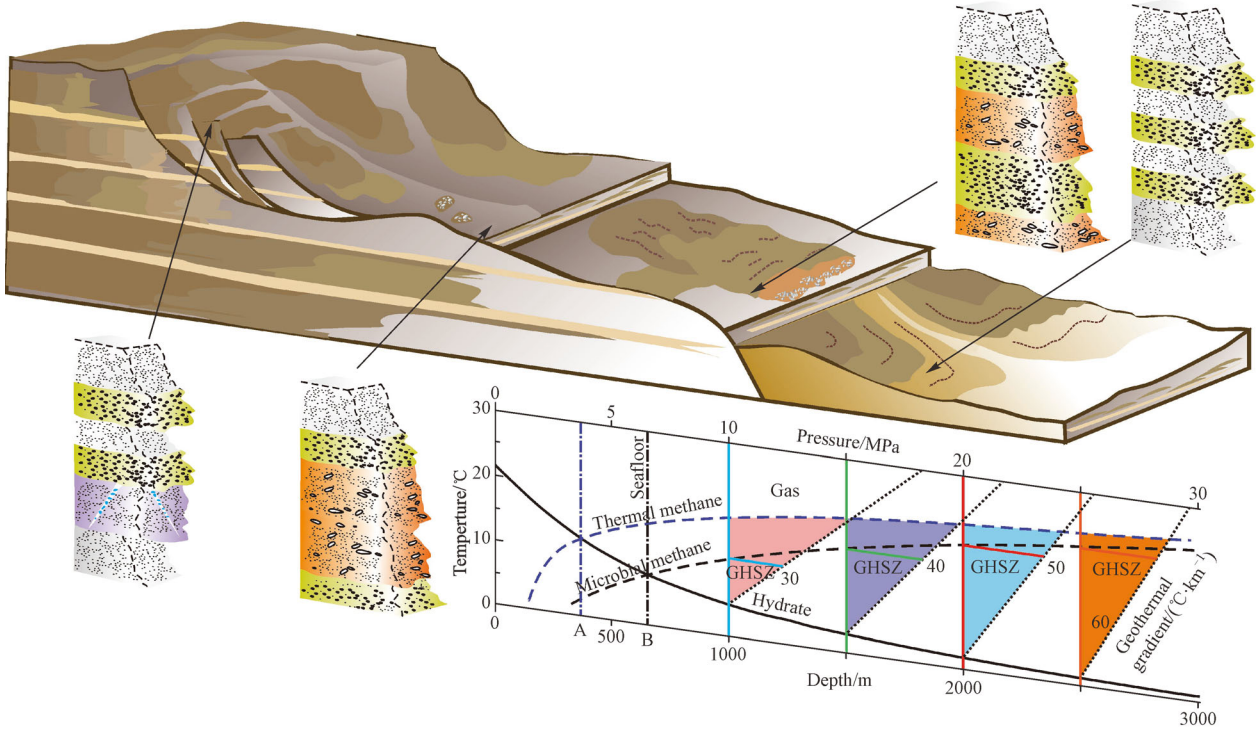

Fig. 11 The proposed model displays various types of gas hydrate accumulation patterns in the MTCs along the slope. At the high dip-angle area in the slope, the MTCs are broken by the normal fault, which forms fractures and a fracture-filling gas hydrate reservoir. In the middle of the slope, owing to the local uplift, the extrusion MTC develops many thrust faults at the toe part. This type of MTC develops a thick pore-filling gas hydrate at the headwall and fracture-filling gas hydrate at its toe. The shear-type MTCs, controlled by bottom flow and gravity, develop a thin-layer pore-filling gas hydrate. The chart given below, modified from Yu et al. (2013), shows the pressure-temperature range in the different parts of the MTCs.

Flow rate: Gas hydrate cannot be formed under the high flow-rate condition because the flow can dissolve free gas and lead to the release of the gas hydrate. According to Wang et al. (2017), if the flow rate of the bottom flow exceeds 10 cm/a, the geothermal value fluctuates. Vadakkepuliyambatta et al. (2015) conducted a study on the Barronian sea hydrate-rich zone and indicated that the dissolved free gas accelerates the release of the gas hydrate because the chemical reaction balance is reversible. Thus, the fierce hydrodynamic environment leads to the release of the gas hydrate and can only form thin-layer pore-filling gas hydrates.

7 Conclusions

1) Integrating the seismic-data interpretation and core log analysis, we classified MTCs into different types according to their stress distribution: tension, extrusion, and shear.

2) The study determines that gas hydrate accumulation varies between the different types of MTCs owing to their kinemics difference within various parts of the MTCs, such as the headwall, translational, and toe areas. Accordingly, we determined the area(s) of gas hydrate accumulation for various types of MTCs. The gas hydrate-bearing reservoir in the tension MTCs, with low hydrate abundance, is mostly located at the toe and headwall. Regarding the extrusion MTCs, the translational and toe areas are favorable reservoir locations for the gas hydrate accumulation. The shear MTCs' headwall and toe parts have coarse-grained sediments, which further favor the gas-hydrate accumulation.

3) From the presented data, the sedimentary and flow erosion rates are the main factors for determining the gas hydrate accumulation in different types of MTCs.

Acknowledgements This research was sponsored by the National 127 Project (No. GZ2011003-05-02-02) and National Natural Science Foundation of China (No. 41572080), as well as the Major State Science and Technology Research Program (No. 2016ZX05024002-002). The authors would like to thank the Guangzhou Marine Geological Survey for providing the geological and seismic data used in this work. We would also like to acknowledge the gas hydrate science team of China University of Geoscience (Beijing).

References

Alves T M, Tiago M, LORENCO, Sérgio, D N (2010). Geomorphologic features related to gravitational collapse: submarine land sliding to lateral spreading on a Late Miocene-Quaternary slope (SE Crete, eastern Mediterranean). Geomorphology, 123(1): 13–33

Alves T M (2015). Submarine slide blocks and associated soft-sediment deformation in deep-water basins: a review. Mar Pet Geol, 67: 262–285

Bouma A H.(1962). Sedimentology of Some Flysch Deposits. Amsterdam: Elsevier, 1–168

Brown H E, Holbrook W S, Hornbach M J, Nealon J (2006). Slide structure and role of gas hydrate at the northern boundary of the Storegga Slide, offshore Norway. Mar Geol, 229(3–4): 179–186

Bryn P, Berg K, Forsberg C F, Solheim A, Kvalstad T J (2005). Explaining the Storegga slide. Mar Pet Geol, 22(1–2): 11–19

Bull S, Cartwright J, Huuse M, 2009. A review of kinematic indicators from mass-transport complexes using 3D seismic data. Mar Pet Geol, 26(7): 1132–1151

Bünz S, Mienert J, Berndt C (2003). Geological controls on the Storegga gas-hydrate system of the mid-Norwegian continental margin. Earth Planet Sci Lett, 209(3–4): 291–307

Cook A E, Goldberg D, Kleinberg R L (2008). Fracture-controlled gas hydrate systems in the northern Gulf of Mexico. Mar Pet Geol, 25(9): 932–941

Chen H, Xie X, Van Rooij D, Vandorpe T, Su M, Wang D (2014). Depositional characteristics and processes of alongslope currents related to a seamount on the northwestern margin of the Northwest Sub-Basin, South China Sea. Mar Geol, 355: 36–53

Daigle H, Dugan B (2010). Origin and evolution of fracture-hosted methane hydrate deposits. J Geophys-Res Sol Ea, 115(B11)

Gee M J R, Gawthorpe R L, Friedmann J S, 2005. Giant striations at the base of a submarine landslide. Mar Geol, 214(1): 287–294

Guan J, Liang D, Wu N, Fan S (2009). The methane hydrate formation and the resource estimate resulting from free gas migration in seeping seafloor hydrate stability zone. J Asian Earth Sci, 36(4–5): 277–288

He Y, Xie X, Kneller B C, Wang Z, Li X (2013). Architecture and controlling factors of canyon fills on the shelf margin in the Qiongdongnan Basin, northern South China Sea. Mar Pet Geol, 41: 264–276

Horozal S, Lee G H, Yi B Y, Yoo D G, Park K P, Lee H Y, Kim W, Kim H J, Lee K (2009). Seismic indicators of gas hydrate and associated gas in the Ulleung Basin, East Sea (Japan Sea) and implications of heat flows derived from depths of the bottom-simulating reflector. Mar Geol, 258(1–4): 126–138

Kvalstad T J, Andresen L, Forsberg C F, Berg K, Bryn P, Wangen M (2005). The Storegga slide: evaluation of triggering sources and slide mechanics. Mar Pet Geol, 22(1–2): 245–256

Lee J W, Kwon K K, Azizi A, Oh H M, Kim W, Bahk J J, Lee D H, Lee J H (2013a). Microbial community structures of methane hydrate-bearing sediments in the Ulleung Basin, East Sea of Korea. Mar Pet Geol, 47(11): 136–146

Lee J Y, Kim G Y, Kang N K, Yi B Y, Jung J W, Im J H, Son B K, Bahk J J, Chun J H, Ryu B J, Kim D S (2013b). Physical properties of sediments from the Ulleung Basin, East Sea: results from second Ulleung Basin gas hydrate drilling expedition, East Sea (Korea). Mar Pet Geol, 47(11): 43–55

Lee M W, Collett T S (2012). Pore- and fracture-filling gas hydrate reservoirs in the Gulf of Mexico Gas hydrate joint industry project leg II Green Canyon 955 H well. Mar Pet Geol, 34(1): 62–71

Matsumoto R, Ryu B J, Lee S R, Lin S, Wu S, Sain K, Pecher I, Riedel M (2011). Occurrence and exploration of gas hydrate in the marginal seas and continental margin of the Asia and Oceania region. Mar Pet Geol, 28(10): 1751–1767

Maslin M, Mikkelsen N, Vilela C, Haq B (1998). Sea-level and gas-hydrate controlled catastrophic sediment failures of the Amazon Fan. Geology, 26(12): 1107–1110

Mienert J, Posewang J (1999). Evidence of shallow- and deep-water gas hydrate destabilizations in North Atlantic polar continental margin sediments. Geo-Mar Lett, 19(1–2): 143–149

Milkov A V, Sassen R (2001). Estimate of gas hydrate resource, northwestern Gulf of Mexico continental slope. Mar Geol, 179(1–2): 71–83

Milkov A V, Sassen R (2000). Thickness of the gas hydrate stability zone, Gulf of Mexico continental slope. Mar Pet Geol, 17(9): 981–991

Nguyen M T, Amtawong J, Smoll K, Chanez A, Yamano M, Dinh G B H, Sengupta S, Martin R W, Janda K C (2016). Gas flow rate and temperature dependence of the Kinetics of Difluoromethane Clathrate Hydrate Formation from CF_2H_2 gas and ice particles. J Phys Chem C, 120(16): 8482–8489

Plaza-Faverola A, Bünz S, Mienert J (2012). The free gas zone beneath gas hydrate bearing sediments and its link to fluid flow: 3-D seismic imaging offshore mid-Norway. Mar Geol, 291–294(4): 211–226

Postma G, Cartigny M J B (2014). Supercritical and subcritical turbidity currents and their deposits—a synthesis. Geology, 42(11):987–990

Riedel M, Collett T S, Park K (2008). Massive gas hydrate occurrences in fractured systems: combined observations from deep drilling campaigns at the Cascadia margin, Krishna-Godhavari Basin, and Ulleung Basin. J Acoust Soc Am, 123(5): 3564

Riestenberg D, West O, Lee S, MacCallum S, Phelps T J (2003). Sediment surface effects on methane hydrate formation and dissociation. Mar Geol, 198(1–2): 181–190

Rothwell R G, Thomson J, Kähler G (1998). Low-sea-level emplacement of a very large Late Pleistocene 'megaturbidite' in the western Mediterranean Sea. Nature, 392(6674): 377–380

Sha Z, Liang J, Zhang G, Yang S, Lu J, Zhang Z, McConnell D R, Humphrey G (2015). A seepage gas hydrate system in northern South China Sea: seismic and well log interpretations. Mar Geol, 366: 69–78

Shankar U, Riedel M (2010). Seismic and heat flow constraints from the gas hydrate system in the Krishna-Godavari Basin, India. Mar Geol, 276(1–4): 1–13

Shi X, Qiu X, Xia K, Zhou D (2003). Characteristics of surface heat flow in the South China Sea. J Asian Earth Sci, 22(3): 265–277

Su M, Hsiung K H, Zhang C, Xie X, Yu H S, Wang Z (2015). The linkage between longitudinal sediment routing systems and basin types in the northern South China Sea in perspective of source-to-sink. J Asian Earth Sci, 111: 1–13

Su M, Sha Z, Qiao S, Liang J, Liu J, Yang R, Wu N (2015). Identification of re-deposited sediments and the relationships with heterogeneous distributions of gas hydrates in the Shenhu area. Acta Geol Sin-Engl, 89(1): 270–272

Su M, Sha Z, Zhang C, Wang H, Wu N, Yang R, Liang J, Qiao S, Cang X, Liu J (2017). Types, characteristics and significances of migrating pathways of gas-bearing fluids in the Shenhu area, northern continental slope of the South China Sea. Acta Geol Sin-Engl, 91 (1): 219–231

Sun Q, Cartwright J, Lüdmann T, Wu S, Yao G (2017). Three-dimensional seismic characterization of a complex sediment drift in the South China Sea: evidence for unsteady flow regime. Sedimentology, 64(3): 832–853

Sun Q, Cartwright J, Wu S, Zhong G, Wang S, Zhang H (2016). Submarine erosional troughs in the northern South China Sea: evidence for Early Miocene deepwater circulation and paleoceanographic change. Mar Pet Geol, 77: 75–91

Sun Q, Cartwright J, Xie X, Lu X, Yuan S, Chen C (2018). Reconstruction of repeated Quaternary slope failures in the northern South China Sea. Mar Geol, 401: 17–35

Tang X, Yang S, Zhu J, Long Z, Jiang G, Huang S, Hu S (2017). Tectonic subsidence of the Zhu 1 Sub-basin in the Pearl River Mouth Basin, northern South China Sea. Front Earth Sci, 11(4): 729–739

Vadakkepuliyambatta S, Hornbach M J , Bünz S, Phrampus B J (2015). Controls on gas hydrate system evolution in a region of active fluid flow in the SW Barents Sea. Ma Pet Geol, 66: 861–872

Vadakkepuliyambatta S, Chand S, Bünz S (2017). The history and future trends of ocean warming-induced gas hydrate dissociation in the SW Barents Sea. Geophys Res Lett, 44(2): 835–844

Wang X, Sain K, Satyavani N, Wang J, Ojha M, Wu S (2013). Gas hydrates saturation using geostatistical inversion in a fractured reservoir in the Krishna-Godavari Basin, offshore eastern India. Mar Pet Geol, 45(4): 224–235

Wang X, Collett T S, Lee M W, Yang S, Guo Y, Wu S (2014). Geological controls on the occurrence of gas hydrate from core, downhole log, and seismic data in the Shenhu area, South China Sea. Mar Geol, 357: 272–292

Yu X, Wang J, Shengli L I, Fang J, Jiang L, Cong X, Liang J, Sha Z (2013). The relationship between tectonic subsidence and BSR of Upper Neogene in the deep-water area of the northern continental slope, South China Sea. Acta Geol Sin-engl, 87(3): 804–818

Yu X, Wang J, Liang J, Li S, Zeng X, Li W (2014). Depositional characteristics and accumulation model of gas hydrates in northern South China Sea. Mar Pet Geol, 56(3): 74–86

Zhong G, Liang J, Guo Y, Kuang Z, Su P, Lin L (2017). Integrated core-log facies analysis and depositional model of the gas hydrate-bearing sediments in the northeastern continental slope, South China Sea. Mar Pet Geol, 86: 1159–1172

Zhou Q, Hu G, Sun Y, Liu X, Song Y, Dong L, Dong C, (2017). Numerical research on evolvement of submarine sand waves in the Northern South China Sea. Front Earth Sci, 11(1): 1–11

Zhou W, Wang Y, Gao X, Zhu W, Xu Q, Xu S, Cao J, Wu J (2015). Architecture, evolution history and controlling factors of the Baiyun submarine canyon system from the middle Miocene to Quaternary in the Pearl River Mouth Basin, northern South China Sea. Mar Pet Geol, 67: 389–407

Zhu M, Graham S, Pang X, McHargue T (2010). Characteristics of migrating submarine canyons from the middle Miocene to present: implications for paleoceanographic circulation, northern South China Sea. Mar Pet Geol, 27(1): 307–319